Revista Mexicana de Astronomía y Astrofísica, **51**, 149–162 (2015)

CONSTRAINTS ON THE NEUTRINO MAGNETIC DIPOLE MOMENT: THE TIP-RGB LUMINOSITY OF GLOBULAR CLUSTERS

S. Arceo-Díaz,[1] K.-P. Schröder,[1] K. Zuber,[2] and D. Jack[1]

Received June 2 2014; accepted March 5 2015

RESUMEN

En este trabajo comparamos las predicciones sobre la luminosidad del extremo superior de la rama de gigantes rojas para estrellas de poca masa a partir de modelos estelares construidos con el código de evolución estelar Cambridge-STARS, con la información observacional de 25 cúmulos globulares, parte de la base de datos homogénea más grande en el cercano infrarrojo. Encontramos que 12 cúmulos globulares suficientemente poblados (encabezados por ω Centauri, el más masivo de la galaxia) sugieren $\mu_{12} \leq 2.2 \times 10^{-12}\mu_B$, mientras que la combinación de las incertidumbres de los modelos estelares y de las observaciones establecen $\mu_{12} \leq 2.6 \times 10^{-12}\mu_B$. Finalmente, utilizando espectros sintéticos construidos con el código PHOENIX para atmósferas estelares, estimamos cualitativamente el efecto de μ_ν en el brillo de bandas específicas en el cercano infra-rojo.

ABSTRACT

In this work we compared the predictions about the tip-RGB bolometric luminosity of low-mass stars in stellar models built with the Cambridge-STARS code for stellar evolution, with the evidence provided by the observational data of 25 globular clusters from the largest homogeneous database in the NIR. We found that 12 well populated globular clusters (headed up by ω Centauri, the largest globular cluster in the galaxy) suggest $\mu_{12} \leq 2.2 \times 10^{-12}\mu_B$, while the uncertainties of both the stellar models and the observations require the more robust constraint $\mu_{12} \leq 2.6 \times 10^{-12}\mu_B$. Finally, using synthetic spectra constructed with the PHOENIX code for stellar atmospheres, we qualitatively estimated the effect on the brightness of specific NIR-bands.

Key Words: globular clusters: general — neutrinos

1. INTRODUCTION

Processes that emit neutrinos from stellar interiors are common ingredients in astrophysics. Although they are mostly known as by-products of nuclear reactions in main-sequence stars, neutrinos are also produced by thermal reactions, involving their weak coupling with electrons in further evolutionary phases. The main processes involving the production of thermal neutrinos are: the photo-, bremsstrahlung-, pair- and plasma-neutrino processes (see Beaudet et al. 1967, for a review). Plasmon decay, first described by Adams et al. (1963), is, in fact, the most important source of thermal neutrinos for the densities and temperatures of degenerate cores inside red giants, near the He-flash.

In recent years, it has been shown that neutrinos have a non-vanishing rest mass and, thus, a variety of new properties, such as electromagnetic moments. Within the Standard Model, the neutrino magnetic dipole moment μ_ν can be calculated at the one loop level to be:

$$\mu_\nu = \frac{3eG_F}{8\sqrt{2}\pi^2} m_\nu = 3.2 \times 10^{-19} \left(\frac{m_\nu}{\mathrm{eV}}\right) \mu_B, \qquad (1)$$

where m_ν and μ_B are the mass of the neutrino flavor and Bohr's magneton respectively (Lee & Shrock 1977; Marciano & Sanda 1977; Fujikawa & Shrock 1980). Though this quantity is too small to be observed in current experiments, it has been proposed since the early 60's (see, Bernstein et al.1963) that it could play an important role in the thermal struc-

[1]Departamento de Astronomía, Universidad de Guanajuato.

[2]Institut für Kern- und Teilchenphysik.

ture and evolution of red giant stars, since a non-zero μ_ν would lead to an enhanced (non-standard) rate of plasmon decay into low-energy neutrino-anti-neutrino pairs, increasing their energy losses considerably.

The study of the consequences of non-standard plasmon decay on the evolution of red giants began with Raffelt & Dearborn (1988). Later, using the luminosity difference between the tip of the red giant branch (tip-RGB) and RR Lyrae stars on the horizontal branch (HB) of globular clusters, they showed that a neutrino dipole moment $\mu_\nu \geq 3 \times 10^{-12}\mu_B$ would surpass the observational constraints (Raffelt et al. 1990). Afterwards, multiple studies supported and, in recent years, improved that value (Raffelt & Weiss 1992; Haft et al. 1994; Viaux et al. 2013) by using more precise prescriptions for plasmon decay and improved photometric data. The most recent constraint is $\mu_\nu \leq 2.6$ (4.5) $\times 10^{-12}\mu_B$, at the 68% (95%) confidence level (Viaux et al. 2013), with stellar tracks predicting observable consequences on the tip-RGB in globular clusters. Since the current experimental limit is: $\mu_\nu \approx 2.9 \times 10^{-11}\mu_B$ (95% CL), found by Beda et al. (2013), stellar astrophysics still provides the best, theoretical, constraint on the neutrino magnetic dipole moment.

In this work, we assessed how a non-zero magnetic dipole moment enhances the production of neutrinos from plasmon decay, changing the thermal structure and evolution of stellar models and increasing the tip-RGB bolometric luminosity over its canonical level. Afterwards, we compared our tip-RGB models with the photometry, in the near infrared, of 25 globular clusters from the database gathered by the group of Ferraro, Valenti and Origlia (Ferraro et al. 2000, 2006, Valenti et al. 2004 a&b, 2007 and 2009) and with the photometric survey of ω Centauri collected by Sollima et al. (2004). We found that our constraint $\mu_\nu \leq 2.2 \times 10^{-12}\mu_B$ (Arceo et al. 2014, 2015) sets the tip-RGB above or at the upper limit of the observational error bars for 12 out of the 25 globular clusters, which were those that showed the best agreement between the observational tip-RGB and the empirical calibration of Valenti et al. (2004). However (§ 2.4 and Figure 3), the combined effect of the statistical uncertainty due the low population density in the remaining clusters and the possible systematical uncertainty of stellar models due to conductive opacities (Cassisi et al. 2007), as well as the $N14 + p$ reaction rates (Weiss et al. 2005) would require $\mu_\nu = 2.6 \times 10^{-12}\mu_B$ to make the non-standard increase in bolometric luminosity observable. Finally, for the first time, we used bolometric corrections and synthetic spectra constructed using the PHOENIX code (Hauschildt 1992) to predict what would be the relative changes on the tip-RGB spectra between canonical ($\mu_\nu = 0$) and non-standard models, with a non-zero magnetic dipole moment, representing RGB stars near the helium-flash in ω Centauri and 47 Tucanae, as well as the possible changes in the brightness on specific NIR-bands.

2. STELLAR MODELS

We used the Cambridge code for stellar evolution (also known as STARS) to construct our models (see Eggleton et al. 1971). Our present version follows Pols et al. (1995) for the prescription of the equation of state, nuclear reaction rates (Caughlan & Fowler 1985) and electron conductivity (Itoh et al., 1983). Opacity tables were updated, specifically for the Eggleton code, by Chen & Tout in 2007, following OPAL 96 (Iglesias & Rogers 1996), for $\log_{10} T/K > 3.95$ and Alexander & Ferguson (1994) in the opposite range.

Like other versions of the STARS code, ours calculated neutrino emissivity by thermal processes using the formulae of Itoh et al. (1992). However, we modified the formula related to the plasma-neutrino process in order to achieve better accuracy and to make it possible to select between the former prescription by Itoh et al. (1992) and the more recent results by Haft et al. (1994) and Kantor & Gushakov (2007). Following the discussion by Valcarce et al. (2012), we selected the fitting formula by Haft et al. (1994), since it provided an accuracy better than 5% in regions of the ρ-T plane in which the degenerate helium cores of low-mass stars are located.

In order to include the contribution of non-standard plasmon decay due to a non-zero magnetic dipole moment, we modified the canonical emissivity, ϵ_{pl}, accordingly to Raffelt et al. (1992):

$$\epsilon_{pl} = F_{SM} Q_{pl} \left(1 + \frac{F_{\mu_\nu}}{F_{SM}}\right). \quad (2)$$

The coefficient F_{SM} (from the Standard Model) contains the Weinberg angle and the number of neutrino flavors, because plasmon decay is completely dominated by the vector component of neutral interactions. The coefficient for non-standard neutrino emission is F_{μ_ν}, and its value depends mostly on the parametrized magnetic dipole moment: $\mu_{12} = \mu_\nu/(10^{-12}\mu_B)$, where μ_B is Bohr's

magneton. F_{μ_ν} is given by:

$$F_{\mu_\nu} = 0.0713\left[\left(\frac{\mu_e}{2\rho_6}\right)^2 + 0.641\left(\frac{\mu_e}{2\rho_6}\right)^{4/3}\right]^{1/2}\mu_{12}^2, \quad (3)$$

where ρ_6 represents matter density, in units of 10^6 g cm^{-3}, and μ_e is the molecular weight.

Of course, there are many standard physical ingredients affecting the mass of the helium core at the tip-RGB (such as opacity tables, the α parameter from mixing-length theory, conductive opacities and, logically, initial helium abundance) that might compete with the effect of a non-zero μ_ν. In § 2.4 we assessed the theoretical error in the values on the tip-RGB luminosity of our models due to the selection of specific values for these parameters.

Below we describe how non-standard neutrino emission affects the calibration of the mass-loss rate. To represent mass-loss due to non-dust driven winds, we used the reinterpretation of the Reimers formula by Schröder et al. (2005). Although there are other prescriptions (Cranmer & Saar 2011), we selected this formula because of its generality, since it can be applied to any stellar model without requiring knowledge of the specific characteristics of each star, and it is also in good agreement with observational data (see for example Schröder et al., 2007, where it was tested by reproducing with high accuracy the mass-loss rates of AGB stars in globular clusters). In § 2.3 we present the effects of non-standard plasmon decay on the calibration of the Reimers mass-loss rate.

2.1. *Defining the tip-RGB*

We chose helium luminosity as our measurement scale to compare models near the helium-flash. As discussed by Arceo et al. (2015), the theoretical tip-RGB in our models was reached when the rate of energy generation by the 3-α process took helium luminosity to around ten solar luminosities ($L_{He} \sim 10L_\odot$).

In Table 1 we compare helium-core masses and bolometric luminosities of stellar tracks during the RGB with the initial values $M_i = 1M_\odot$, four different initial metallicities: $Z_i = 0.0001, 0.001, 0.01$ and 0.02 and helium abundance expressed as: $Y_i = 0.24 + 2Z_i$ (according to the prescription by Pols et al., 1998). Each column shows these two parameters for models with specific helium luminosities. We selected four values for L_{He} : $0.1L_\odot, 1L_\odot$, $10L_\odot$ and $100L_\odot$ to probe the effect of a specific selection of L_{He} on the corresponding bolometric luminosity. The four sets of models showed the same tendency: a significant increase of bolometric luminosity (around 300 to $400L_\odot$) between the models with $L_{He} = 0.1L_\odot$ and $L_{He} = 10L_\odot$. After this, as shown in Figure 1, the bolometric luminosity remained almost unchanged (varying less than $10L_\odot$), while the helium luminosity increased rapidly towards the He-flash. This marked the maximum luminosity for any stellar track before the helium flash, which was completely dominated by the physical parameter controlling the mass of the degenerate helium core.

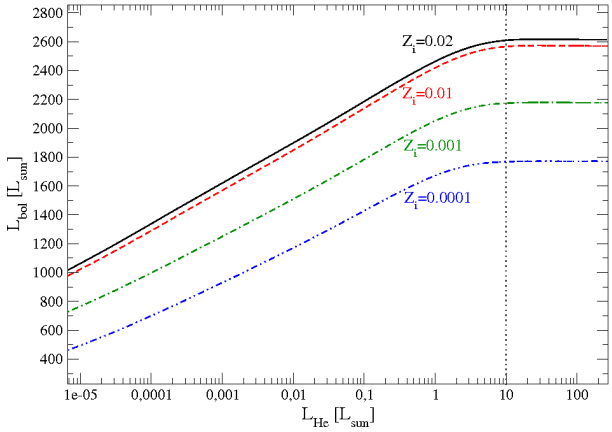

Fig. 1. Bolometric luminosity versus helium luminosity during the last million years before the helium flash, for tracks with $M_i = 1.0M_\odot$ and four different metallicities. The bolometric luminosity becomes almost independent of the increment in the energy generation by the 3-α process after $L_{He} = 10L_\odot$.

The existence of a threshold of bolometric luminosity gave us an advantage when measuring the effects of non-standard neutrino emission. Once the standard ingredients have been properly calibrated, any increase in energy loss during the degenerate phase of the helium core means a larger core mass and an increased bolometric luminosity. Thus, if the non-standard decay rate of plasmons is high enough, it results in noticeable changes in bolometric luminosity that could not be reached by standard processes for any stellar track with a known chemical composition.

One important point in our analysis was to check if the non-standard increase in core mass would show any dependence on their proximity to the He-flash. Analyzing the models in Table 1, and their corresponding analogs which include non-zero values for μ_{12}, we found that, for any set of models with equal helium luminosity, δM_c depends mostly on the assumed value for μ_{12} (with small variations depending on the metallicity, as we showed in § 2.3). Hence,

TABLE 1

CORE MASS AND LUMINOSITY OF RGB MODELS*

$Z = 0.0001$	$L_{He} = 0.1L_\odot$	$L_{He} = 1L_\odot$	$L_{He} = 10L_\odot$	$L_{He} = 100L_\odot$
$M_c[M_\odot]$	0.4782	0.4924	0.4983	0.4984
$L[L_\odot]$	1432	1679	1771	1772
$Z = 0.001$	$L_{He} = 0.1L_\odot$	$L_{He} = 1L_\odot$	$L_{He} = 10L_\odot$	$L_{He} = 100L_\odot$
$M_c[M_\odot]$	0.4693	0.4822	0.4883	0.4888
$L[L_\odot]$	1790	2057	2175	2177
$Z = 0.01$	$L_{He} = 0.1L_\odot$	$L_{He} = 1L_\odot$	$L_{He} = 10L_\odot$	$L_{He} = 100L_\odot$
$M_c[M_\odot]$	0.4595	0.4717	0.4783	0.4789
$L[L_\odot]$	2145	2438	2585	2589
$Z = 0.02$	$L_{He} = 0.1L_\odot$	$L_{He} = 1L_\odot$	$L_{He} = 10L_\odot$	$L_{He} = 100L_\odot$
$M_c[M_\odot]$	0.4537	0.4658	0.4721	0.4728
$L[L_\odot]$	2207	2498	2644	2649

*Tabulated values correspond to stellar tracks with $M_i = 1M_\odot$, at different stages of the on-setting of helium burning and for four different metallicities. Bolometric luminosity, practically, does not increase beyond $L_{He} = 10L_\odot$.

our choice of where exactly (in terms of the magnitude of L_{He}) to put our theoretical tip-RGB did not have any influence on the constraint derived for the neutrino cooling and, hence, its dipole moment. Because of its sufficient proximity to the He-flash, we defined our tip-RGB from a model that reached $L_{He} = 10L_\odot$.

2.2. *Non-standard cooling and its effect on the stellar core*

The scenario discussed above holds if one considers non-standard plasmon decay into neutrino pairs, the only difference being a higher degree of cooling inside the degenerate helium core. This enhanced cooling is what eventually led to an observable increase in bolometric luminosity, whose magnitude was used to constrain the magnetic dipole moment of neutrinos. During the ascent to the RGB, plasmon decay was the main cooling process inside the increasingly compact helium core. As more thermal energy was taken away by neutrino pairs, the helium flash was delayed, allowing, in the mean time, the accretion of more helium from the hydrogen-burning shell above the core (this, in turn, increased the density, enhancing plasmon decay and creating a feedback effect). As the core becomes more compact and cooler, the stellar bolometric luminosity grows rapidly as more photons, produced by hydrogen shell burning, are released towards the upper layer of the stellar envelope.

Since we only included the effect of μ_ν on the decay rate of plasmons into neutrino pairs, the changes in the emission rate of neutrinos for the other (nuclear and thermal) processes came from a feedback effect. Even so, it is worthwhile to state in which manner the existence of a non-zero magnetic dipole moment affected the thermal structure of the red giant. Figure 2 illustrates this for a stellar track with $M_i = 1M_\odot$ and $Z = 0.02$. The left panel shows the temporal evolution of the peak luminosity for each of the several processes that produce neutrinos in the stellar interior (instead of explicitly showing age in years, we normalized it as the time when the tip-RGB was reached). Non-standard models differed greatly from the canonical scenario as the production of neutrinos by plasmon decay was, abruptly turned on and quickly surpassed the photo neutrino process (its intensity strongly depending on μ_ν; e.g. non-standard models differ from the canonical scenario by almost three orders of magnitude for $\mu_{12} \geq 1$). The right panel shows neutrino luminosity at the tip-RGB. Here we see the scenario described by Kippenhahn & Weigert 1990): the peak of neutrino luminosity coincided with the ignition point of the 3-α process. The neutrino luminosity caused by thermal processes was almost twice its canonical value for our model with $\mu_{12} = 2.2$ (see Table 2). Outside the core, neutrino luminosity, caused by the multiple stages of the CNO cycle taking place in the H-burning shell, increased due to the stronger grav-

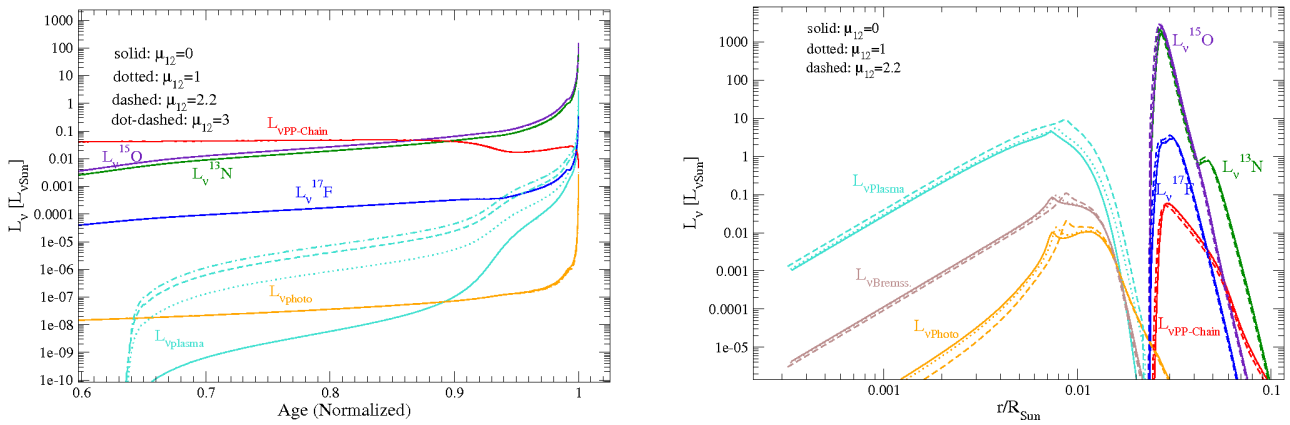

Fig. 2. Comparison of neutrino luminosity during the RGB between the canonical scenario and non-standard tracks. The left panel shows the temporal evolution of the luminosity peak of each channel (with the age normalized to 1 at the tip-RGB), while the right panel shows neutrino luminosity versus radius at the tip-RGB. The initial mass and metallicity of these tracks are $M_i = 1.0 M_\odot$ and $Z = 0.02$.

TABLE 2

NUCLEAR AND THERMAL PROCESSES CONTRIBUTIONS TO TOTAL NEUTRINO LUMINOSITY*

$1.0M_\odot$	$\mu_{12}=0$	$\mu_{12}=1$	$\mu_{12}=2.2$	$\mu_{12}=3$
L_ν $[L_{\nu\odot}]$	6467	6800	7780	8633
$L_{\nu PP}/L_\nu$	3.04(-5)	2.80(-5)	2.18(-5)	2.17(-5)
$L_{\nu CNO}/L_\nu$	0.994	0.993	0.990	0.987
$L_{\nu Th}/L_\nu$	5.73(-3)	6.73(-3)	9.95(-3)	1.27(-2)
$L_{\nu pl}/L_{\nu Th}$	0.981	0.985	0.990	0.993

*For a tip-RGB model with $1M_\odot$ and $Z = 0.02$.

itational pull of a more compact helium core. Although these variations appeared to be small, their effect was large enough to cause a noticeable increase in bolometric luminosity. We discuss this next, using the models of Table 3.

2.3. *Realistic stellar models with non-standard cooling*

The changes induced by non-standard neutrino emission affected not only the mass of the degenerate core and the bolometric luminosity but also other stellar parameters more related to the envelope (namely, the mass-loss rate, effective temperature, and stellar radius). We discuss such changes below.

We selected four sets of tracks with metallicities: $Z = 0.0001, 0.001$, 0.01 and 0.02, as representative of stars within globular clusters throughout the galactic bulge and halo. In each set, we compared the canonical tip-RGB with that for which we assumed $\mu_{12} = 1.5, 2.2$ or 2.6. Although we only present tip-RGB models of stellar tracks in which the initial mass was $1M_\odot$, the results are qualitatively similar when other values are assumed.

Even if the mass-loss rate did not alter tip-RGB bolometric luminosity (Castellani & Castellani 1993), a proper recalibration of the mass-loss parameter η was necessary when considering non-standard neutrino emission; otherwise the resulting speed-up of nuclear reactions, happening inside the hydrogen burning shell, could lead to an accelerated stellar expansion leaving a helium white dwarf (Arceo et al. 2013). Table 3 shows the value of η (first row in each set) necessary to obtain the same envelope mass (second row) in the canonical scenario. We found that: (a) for each specific μ_{12}, a single η reproduced the tip-RGB mass of the canonical scenario, with a very small dependence on the initial metallicity. (b) Increasing μ_{12} required a reductiojn of η by some non-negligible amount to reproduce the tip-RGB mass of the canonical models (e.g. while our model with $\mu_{12} = 1.5$ only needed η to be reduced by around 15%, the one with $\mu_{12} = 2.6$ agreed only if η was reduced by almost 50%).

From the third to the fifth row of each set, we show the mass of the degenerate core (M_c), its non-standard increase (δM_c) when different μ_{12} are assumed and the corresponding bolometric luminosity (L_{bol}). Overall, we found the same tendency as of previous works (Raffelt 1990 a&b, 1992, Viaux et al. 2013): increasing values for μ_{12} led to larger core

TABLE 3

TIP-RGB MODELS WITH BOTH MASS-LOSS AND A NON-ZERO μ_ν*

$Z = 0.0001$	$\mu_{12} = 0$	$\mu_{12} = 1.5$	$\mu_{12} = 2.2$	$\mu_{12} = 2.6$
$\eta_{14}[M_\odot yr^{-1}]$	8.00	6.50	5.60	5.10
$M_*[M_\odot]$	0.8889	0.8885	0.8840	0.8822
$M_c[M_\odot]$	0.4983	0.5124	0.5236	0.5297
$\delta M_c[M_\odot]$	0.0	0.0141	0.0253	0.0314
$L_{bol}[L_\odot]$	1772	2104	2409	2591
$L_\nu[L_\odot]$	127	153	176	189
$T_{eff}[K]$	4195	4155	4124	4107
$R_*[R_\odot]$	80	89	97	101

$Z = 0.001$	$\mu_{12} = 0$	$\mu_{12} = 1.5$	$\mu_{12} = 2.2$	$\mu_{12} = 2.6$
$\eta_{14}[M_\odot yr^{-1}]$	8.00	6.50	5.60	5.10
$M_*[M_\odot]$	0.8424	0.8429	0.8431	0.8425
$M_c[M_\odot]$	0.4891	0.5004	0.5099	0.5154
$\delta M_c[M_\odot]$	0.0	0.0113	0.0208	0.0263
$L_{bol}[L_\odot]$	2179	2497	2791	2974
$L_\nu[L_\odot]$	157	181	202	216
$T_{eff}[K]$	3796	3748	3704	3676
$R_*[R_\odot]$	108	119	129	135

$Z = 0.01$	$\mu_{12} = 0$	$\mu_{12} = 1.5$	$\mu_{12} = 2.2$	$\mu_{12} = 2.6$
$\eta_{14}[M_\odot yr^{-1}]$	8.00	6.50	5.60	5.10
$M_*[M_\odot]$	0.7459	0.7484	0.7412	0.7490
$M_c[M_\odot]$	0.4794	0.4880	0.4953	0.4988
$\delta M_c[M_\odot]$	0.0	0.0094	0.0159	0.0194
$L_{bol}[L_\odot]$	2573	2847	3107	3252
$L_\nu[L_\odot]$	186	207	226	236
$T_{eff}[K]$	2970	2909	2866	2848
$R_*[R_\odot]$	192	211	227	235

$Z = 0.02$	$\mu_{12} = 0$	$\mu_{12} = 1.5$	$\mu_{12} = 2.2$	$\mu_{12} = 2.6$
$\eta_{14}[M_\odot yr^{-1}]$	8.00	6.50	5.55	4.67
$M_*[M_\odot]$	0.6977	0.7000	0.6992	0.6993
$M_c[M_\odot]$	0.4733	0.4809	0.4877	0.4917
$\delta M_c[M_\odot]$	0.0	0.0076	0.0144	0.0184
$L_{bol}[L_\odot]$	2617	2872	3111	3264
$L_\nu[L_\odot]$	197	206	230	275
$T_{eff}[K]$	2622	2569	2538	2513
$R_*[R_\odot]$	249	271	289	302

*Non-standard neutrino emission leads to larger core masses and bolometric luminosities, accompanied by cooler and larger stellar envelopes.

masses and bolometric luminosities. The values in our models can be parametrized by the fitting formula:

$$M_c = M_{c-std} + \delta M_c, \quad (4)$$

where the canonical mass of the helium core is given by:

$$M_{c-std} = 0.4906 - 0.016M^* - 0.008Z^* - 0.22Y^*, \quad (5)$$

with

$$M^* = M_i - 0.90, \quad (6)$$

$$Y^* = Y_i - 0.25, \quad (7)$$

$$Z^* = 3 + \log_{10} Z_i, \quad (8)$$

(the sub-index i indicates initial values) and the non-standard increase is:

$$\delta M_c = \delta M_\mu (1.0 - 0.21Z^* + 0.14M^*), \quad (9)$$

where

$$\delta M_\mu = 0.0267\left[(\mu_1^2 + \mu_{12}^2)^{0.5} - \mu_1 - (\mu_{12}/\mu_2)^{1.5}\right], \quad (10)$$

with $\mu_1 = 1.2$ and $\mu_2 = 3.3$, as was derived by Raffelt (1990). In addition, the He-core mass-luminosity relationship is:

$$L_{bol} = 1.58 \times 10^5 M_c^6 \times 10^{0.77Y^* + 0.12Z^*}. \quad (11)$$

In this way, equations 4 and 11 approximate core mass and bolometric luminosity (as given by our models) with a maximum percentage error of about 5%, for any stage on the ascent to the RGB, in the plausible range $M_* = 0.8$ - $1.2M_\odot$ for stellar mass, and $Z = 0.0001$ to $Z = 0.02$ (with the initial helium content as a function of metallicity).

2.4. *Impact of the He abundance or other factors?*

Next, we explored the influence of multiple standard ingredients on the mass of the helium core at the tip-RGB, and analyzed which ones could affect the non-standard increase driven by an enhanced plasmon decay (or compete with it by increasing the bolometric luminosity to the same level).

We began with the mass-loss rate. By running stellar tracks analog to those shown in Table 3, without considering mass-loss, we obtained variations of the bolometric magnitude of the tip-RGB smaller than 10^{-3} mag. We thus confirmed the statement by Castellani & Castellani (1993) about the negligible impact of the mass-loss rate on stellar luminosity at the He-flash.

Next, we considered the value of α in convection theory. Throughout our work we had been using $\alpha = 2$, which has been already tested to match the solar case (Pols et al. 1995) and the outer layers of RGB stars in eclipsing binaries and clusters (Pols et al. 1997, 1998, Schröder et al. 1997). However, we tested stellar tracks with variations of about ±20%. We found that while there were important changes on the radius of the envelope and on the effective temperature, the mass of the helium core was not affected. The resulting bolometric luminosity presented variations of 10^{-3} mag. In fact, well-tested models from newer evolution codes, such as that by Pietrinferni et al. (2004, 2006), describe similar tracks. While both factors, mixing length and mass-loss rate, are important for the effective temperature and stellar radius at the tip-RGB, they do not play an important part in the luminosity of canonical or non-standard evolution.

Our current version of the code uses OPAL 96 (Iglesias & Rogers 1996), for $\log_{10} T/K > 3.95$ and Alexander & Ferguson (1994) in the opposite range, as implemented on the Eggleton code by Chen & Tout (2007). Salaris et al. (2002) and Cassisi et al. (2007) raised attention to the conductivity of the electron gas, which controls heat transport and temperature gradient in a degenerate helium core near the tip-RGB. Indeed, this is another element that influences the final core helium mass and the tip-RGB luminosity. For a strongly degenerate electron gas, we employed the conductive opacities of Itoh et al. 1983 (see Pols et al. 1995), which according to Cassisi et al. (2007) represent a large improvement for such conditions. To assess the differences between using OPAL 96 tables or the OPAL, we ran analog models to those in Table 3. Overall, we found that the use of OPAL 92 led to more massive cores ($\delta M_c \approx 0.005 M_\odot$) and larger bolometric luminosities ($\delta L_{bol} \approx 100 L_\odot$). The uncertainty associated with more recent choices of conductive opacities, however, is even smaller and, at worst, is comparable to the uncertainties discussed above.

We also analyzed the variations in tip-RGB luminosity due to initial mass. We took the range from $0.8 M_\odot$ (models with an age comparable to that of the universe) to $1.1 M_\odot$ (models with an age around 5 Gyrs), taking $0.95 M_\odot$ as our central value. Apart from the obvious differences in stellar age, we found that, with small variations due to metallicity (see the table below), the tip-RGB luminosity varied around 0.04 mag with respect to that of the central value.

A more obvious candidate to exert influence on the tip-RGB luminosity may be the initial hydrogen-helium content. In the models presented here, we used the same quasi-solar abundances ($X = 0.70$, $Y = 0.28$, $Z = 0.02$), and a $\Delta Y/\Delta Z = 2$ in non-solar compositions, like the the ones that were carefully tested by Pols et al. (1995 and 1997). To asses the influence of helium composition, we constructed analog models in which the helium mass fraction was arbitrarily changed by ±30% from our benchmark value. We found two important results: (a) only a reduced abundance of helium can raise the bolometric luminosity of the tip-RGB to the same level as that predicted for stellar tracks with a non-zero μ_ν. This, of course, can be ruled out since in some cases more than the primordial helium abundance is needed to rival the effect of dipole moments larger than $\mu_{12} = 2.2$. (b) Helium enrichment blurs out the increase in bolometric luminosity driven by a non-zero μ_ν. We found than in stellar tracks with 30% more helium, reaching the same luminosity level as that provided by $\mu_{12} = 2.2$ required $\mu_{12} = 2.6$ instead.

Apart from the uncertainties related to the selection of the stellar parameters discussed above, there are other two main factors that could affect the final bolometric luminosity of the tip-RGB: the reduction of the mass of the degenerate core due the new conductive opacities (Cassisi et al. 2007) and the new $N14 + p$ reaction rate (Weiss et al. 2005). This two factors could lower the tip-RGB of stellar models by 0.08 and 0.12 mag, respectively. Combining these values quadratically with the lower limit of the error bars in our models we obtained a systematic shift of up to 0.16 mag. In Figure 3 (next section) we compare our canonical and non-standard tip-RGB models, shifted downward by 0.10 and 0.16 mag, with the bolometric luminosity from observations.

3. COMPARISON WITH OBSERVATIONS: THE TIP-RGB LUMINOSITY OF GLOBULAR CLUSTERS

3.1. *Constraint on the magnetic dipole moment based on bolometric luminosities.*

Throughout our previous work (see Arceo et al. 2014, 2015), based on a careful analysis of the stellar populations in the upper two magnitude bins and taking into account the reported chemical spread, we used the observed tip-RGB luminosity of ω Cen to propose the constraint $\mu_\nu \leq 2.2 \times 10^{-12} \mu_B$ on the magnetic dipole moment of neutrinos. In this section, we discuss if this could be supported by the evidence on the color magnitude diagrams of other, less populated, globular clusters.

TABLE 4

VARIATION OF BOLOMETRIC MAGNITUDE DUE TO Y_i, M_i, η AND α*

δM_{bol}	$Z = 0.0001$	$Z = 0.001$	$Z = 0.01$	$Z = 0.02$
$\delta M_{bol}, Y_i^{'} = 1.3Y_i$	0.12	0.08	0.05	0.05
$\delta M_{bol}, M_i \pm 0.15M_\odot$	$\pm^{0.05}_{0.02}$	$\pm^{0.03}_{0,02}$	$\pm^{0.008}_{0.006}$	$\pm^{0.004}_{0.002}$
$\delta M_{bol}, \eta = 0$	0.0001	0.0005	0.007	0.008
$\delta M_{bol}, \alpha_{mix} \pm 0.4$	$\pm^{0.002}_{0.005}$	$\pm^{0.001}_{0.0008}$	$\pm^{0.004}_{0.002}$	$\pm^{0.005}_{0.002}$
$\delta M_{bol}, \mu_{12} = 2.2$	-0.333	-0.269	-0.205	-0.187

*Lines 1 to 4 ordered by decreasing importance. The variation is compared with that coming from assuming $\mu_{12} = 2.2$ (last line). For each metallicity, we evolved a $0.95M_\odot$ RGB-tip model with $Y_i = 0.24 + 2Z_i$, $\eta = 8 \times 10^{-14} M_\odot \mathrm{yr}^{-1}$ and $\alpha_{mixing} = 2.00$.

We gathered a sample of 25 globular clusters from the database of the group of Ferraro, Valenti and Origlia (Ferraro et al. 2000, 2006; Valenti et al., 2004a, 2004b, 2007 and 2010), and from the photometric survey of ω Centauri, collected by Sollima et al. (2004). Being the largest homogeneous near infrared survey of globular clusters in the galactic bulge and halo, this data base provides an accurate estimation of the tip-RGB; the photometry is free of contaminating AGB, variable and field stars. This gave us a fair chance to constrain the magnetic dipole moment of neutrinos using the bolometric magnitude of our stellar models. For each cluster, the photometric data of the brightest, non-variable, star gave an estimation of the tip-RGB and, using the bolometric corrections by Montegriffo et al. (1998), the flux on the NIR bands was translated into the bolometric magnitude M_{bol}^{Tip}. Since for twelve clusters in our sample (marked by an asterisk in Table 5) there were no error bars reported in literature, we created the ones shown in Column 3 by combining the conservative value 0.25 mag. (Valenti et al. 2010), which accounts for the errors in the distance modulus and the reddening, with the statistical uncertainty σ_s (Column 6).

Our strongest requirement for selecting our sample clusters was to deal with the smallest possible statistical uncertainty, minimizing the intrinsic underestimation associated with using the brightest star to probe the theoretical tip-RGB. According to the statistical analysis conducted by Crocker & Rodd (1997, private communication), detailed by Ferraro et al. (2000), we selected clusters with a star count of more than 30 on the upper 2 mag bins, which gave a statistical uncertainty, σ_s, of less than 0.16 mag (lower than the non-standard increase in luminosity for models with $\mu_{12} = 2.2$ or 2.6). In addition, we restricted our sample to clusters in which the majority of RGB stars were over the theoretical ridge line and did not have multiple RGB branches. ω Centauri, being the most populated cluster in the galaxy (thus having the smallest statistical uncertainty), was our only exception to this last requirement (it was shown by several previous works to have multiple stellar populations with different metallicities, e.g. Norris and DaCosta 1995; Pancino et al. 2003). However, it also has been found that around 60% of the measured red giants constitute a main population with [Fe/H] ≈ -1.7 (e.g. Norris & DaCosta 1995; Suntzeft & Kraft 1996; Hilker & Richtler 2000; Sollima et al. 2005; Marino et al. 2008) and that 88% of them have metallicities [Fe/H] $= -1.7 \pm 0.2$ (Johnson & Pilachowski 2010). In this study, we constructed our models for ω Centauri by taking the global metallicity of its main population (equivalent to the global metallicity: $[M/H] = -1.39$).

We ran stellar tracks with $M_i = 0.95M_\odot$, with the mass fraction of metals, Z, matching the reported global metallicity $[M/H]$ for each globular cluster (assuming an α-enhancement of 0.3), and with the mass fractions for hydrogen and helium expressed as functions of Z by the prescription by Pols et al. (1998). We included error bars of 0.05 mag for each point representing a model (see Figure 3), in accordance with our discussion in § 2.4. We considered three sets of tracks: the canonical scenario and those with $\mu_{12} = 2.2$ and 2.6. Then, using the photometric data of each cluster, we compared the bolometric magnitudes of our models looking for cases in which the error bars could constrain the magnetic dipole moment of neutrinos.

As a complementary analysis, we compared our models with the empirical formula obtained by Valenti et al. (2004):

$$M_{empirical}^{Tip} = -3.85 - 0.19[M/H], \qquad (12)$$

TABLE 5

DIFFERENCE BETWEEN THE CALIBRATED AND EMPIRICAL BOLOMETRIC TIP-RGB OF THE SAMPLE AND OUR CANONICAL AND NON-STANDARD ($\mu_{12} = 2.2$) STELLAR MODELS

Cluster	[M/H]	M_{obs}^{Tip}	$M_{emp.}^{Tip}$	N_{*2}	σ_s	δM_0^{Tip}	$\delta M_{2.2}^{Tip}$	$\delta M_{2.2-e}^{Tip}$
ω-Cen.	−1.39	-3.59 ± 0.16	−3.59	310	0.017	+0.01	−0.17	−0.17
NGC6441	−0.52	-3.90 ± 0.20	−3.75	200	0.025	+0.18	−0.06	−0.21
Terzan5*	−0.14	-3.96 ± 0.25	−3.82	180	0.028	+0.09	+0.00	−0.14
M15	−1.91	-3.55 ± 0.20	−3.49	180	0.028	+0.08	−0.23	−0.28
NGC6440	−0.40	-3.82 ± 0.21	−3.77	113	0.044	+0.09	−0.14	−0.19
Terzan2*	−0.53	-3.81 ± 0.26	−3.75	100	0.050	+0.07	−0.15	−0.21
Terzan9*	−1.01	-3.86 ± 0.26	−3.66	90	0.055	+0.21	−0.04	−0.24
Terzan6*	−0.43	-3.89 ± 0.26	−3.77	87	0.056	+0.13	−0.07	−0.19
NGC6273*	−1.21	-3.56 ± 0.26	−3.62	87	0.056	−0.15	−0.39	−0.33
NGC6388*	−0.42	-3.76 ± 0.26	−3.77	86	0.058	+0.04	−0.20	−0.19
47-Tuc.	−0.59	-3.71 ± 0.19	−3.74	80	0.060	+0.00	−0.23	−0.20
NGC6401*	−1.20	-3.42 ± 0.26	−3.62	79	0.062	−0.21	−0.46	−0.26
Djorg2*	−0.45	-3.50 ± 0.26	−3.76	79	0.062	−0.26	−0.46	−0.20
NGC362	−1.15	-2.90 ± 0.21	−3.63	77	0.064	−0.76	−1.01	−0.27
NGC6569	−0.66	-3.59 ± 0.26	−3.72	75	0.064	−0.11	−0.36	−0.23
NGC6255*	−1.43	-3.56 ± 0.26	−3.58	57	0.085	−0.02	−0.29	−0.27
NGC6380	−0.68	-3.88 ± 0.22	−3.77	55	0.090	+0.18	−0.06	−0.17
NGC6266*	−0.80	-3.56 ± 0.27	−3.70	55	0.090	−0.12	−0.36	−0.22
NGC6637	−0.57	-3.34 ± 0.31	−3.74	44	0.110	−0.37	−0.61	−0.21
NGC6293*	−1.55	-3.23 ± 0.28	−3.55	36	0.130	−0.33	−0.60	−0.28
NGC6528*	+0.04	-4.06 ± 0.28	−3.86	36	0.130	+0.28	+0.10	−0.10
M3	−1.16	-3.61 ± 0.24	−3.63	35	0.140	−0.01	−0.27	−0.25
M92	−1.95	-3.64 ± 0.26	−3.48	33	0.150	−0.18	−0.13	−0.29
NGC6638	−0.78	-3.88 ± 0.35	−3.70	32	0.150	+0.20	−0.05	−0.23
NGC6304	−0.56	-3.59 ± 0.33	−3.74	30	0.160	−0.12	−0.36	−0.21

which gives the tip-RGB bolometric magnitude as a function of the global metallicity of the cluster. This empirical formula shows a good agreement with observational data and we used it to estimate the variations of the non-standard increase in bolometric luminosity over the wide range of $[M/H]$ in our sample.

Table 5 shows our comparison between stellar models and observational data. Columns 1 to 6 give the name of each globular cluster, its global metallicity, the observed bolometric magnitude (M_{obs}^{tip}), the empirical estimation (M_{emp}^{Tip}), the number of stars in the upper 2-mag bins (N_{*2mag}) and the statistical uncertainty (σ_s). Columns 7 and 8 show the difference (in bolometric magnitude) between our canonical (δM_0^{Tip}) and non-standard tip-RGB models ($\delta M_{2.2}^{Tip}$) and the observed bolometric magnitude. Column 9 shows the magnitude difference between our non-standard models and the empirical tip.

Over the entire metallicity range, the average observational bolometric tip-RGB was: $\langle M_{obs}^{Tip} \rangle = -3.65$ (with an standard deviation of 0.24 mag), while for our canonical and non-standard models (with $\mu_{12} = 2.2$) we obtained: $\langle M_0^{Tip} \rangle = -3.66$ and $\langle M_{2.2}^{Tip} \rangle = -3.92$ ($\delta M_{bol} = 0.26$), showing a clear tendency to become larger for the less metallic clusters. Thus, the averaged non-standard tip-RGB over the metallicity range in our sample was already more than 1σ away from the averaged tip-RGB of observational data.

The two upper panels in Figure 3 show the comparison between the calibrated M_{obs}^{Tip} (black asterisks), the empirical estimation by Valenti et al. (2004) (green squares), and our canonical (red-circle) and non-standard tip-RGB models with $\mu_{12} \leq 2.2$ (upward-blue triangle) and 2.6 (downward-orange triangle). All our models reproduced the same tendency. M_{obs}^{Tip} did not coincide with $M_{emp.}^{Tip}$ in all cases; some clusters showed better agreement than others. Twelve clusters showed the best match not only between these two models, but also with our canonical models: M15, NGC 6273, 6304, 6266, 6569, 6440, Terzan 2, NGC 6255, ω Cen., M3, 47 Tuc. and Terzan 6 (for the last five, the observational calibrations fell within the 0.05 mag error bars of our canonical models).

We considered three scenarios for all the clusters in our sample, when trying to obtain a constraint on μ_ν: (a) the upper limit of the error bar being smaller than or equal to the bolometric magnitude of our tip-RGB model with $\mu_{12} = 2.2$, (b) the same scenario, but with $\mu_{12} = 2.6$ and (c) the bolometric magnitude of both falling within the observational error bars.

The first scenario for which the observational data suggest that $\mu_{12} \leq 2.2$, is favored by 12 clusters (having raised the upper limit for their error bars below the central value of the bolometric magnitude in the non-standard models in Figure 3), eight of which (ω Cen, M15, M3, 47 Tucanae, NGC 6273, 6266, 6304 and 6569) belonged also to the group showing the best agreement between M_{obs}^{Tip}, $M_{emp.}^{Tip}$ and our theoretical models. Nine of these clusters (see Table 5) had $\sigma_s \leq 0.1$ mag. Among them, ω Cen, M15, NGC 6569 and 47 Tucanae allowed to place the non-standard tip-RGB, with $\mu_{12} = 2.2$, more than $1\sigma_s$ above the upper limit of the error bar.

Four clusters (NGC 6441, 6440, Terzan 2 and 6) belong to the second scenario, in which $\mu_{12} \leq 2.6$ was a better constraint. Although fewer than those in the first scenario, these clusters also showed a rather small statistical uncertainty (all having $\sigma_s \leq 0.06$) and three of them (NGC6440, Terzan 2 and 6) belong to the group of clusters with the best agreement between observation, empirical data and theoretical models.

There were six cases (M92, NGC 6528, 6388, 6380, 6638 and Terzan 9) in which either the best estimation for M_{obs}^{Tip} was too bright (the observational value was much brighter than the empirical calibration) or the uncertainty was sufficiently large to contain both constraints within the error bars. In three globular clusters (NGC 362, 6293 and Terzan 5), the M_{obs}^{Tip} strongly differed from both the empirical estimation and the stellar models. This could indicate possible systematic effects on the observational calibration, that could be affecting, not only these clusters, but also others in our sample. However, we consider that most of the clusters that showed a good degree of agreement between the observational calibration and the empirical formula (both resulting from the work by the group of Valenti, Ferraro & Origlia), can be used in this analysis with less concern.

The middle and lower panels inside Figure 3 show the results of introducing systematical shifts of 0.10 (middle) and 0.16 (bottom), accounting for possible uncertainties in the M_{bol}^{Tip} of our models, due to the new electron conductivity (Cassisi et al. 2005) and the $N14 + p$ reaction rates (Weiss et al. 2005). In these scenarios, a larger magnetic dipole moment was required to pass above the upper level of the observational error bars. In the middle panels, nine clusters allowed to place the constraint $\mu_{12} \leq 2.6$. Only four clusters (ω Cen., NGC 6266, 6569 and 47 Tucanae) suggested the more restrictive value $\mu_{12} = 2.2$. In the two lower panels, we show 10 clusters that allowed to constraint μ_ν. This time only ω Cen, NGC 6401 and Dorg 2 suggested $\mu_{12} \leq 2.2$. As these dimmings of the tip-RGB of our stellar models represent only marginal, but possible, effects, due the systematical uncertainties, the constraint $\mu_{12} \leq 2.6$ is a more robust upper limit when considering the data from the observational calibration of most clusters in our sample.

The NIR-database by Valenti, Ferraro and Origlia (2004a, 2004b, 2007, 2010), along with the photometric survey on ω-Cen by Sollima et al. (2004), gave us a fair chance of constraining the magnetic dipole moment of neutrinos. Overall, eleven globular clusters showed not only a low statistical uncertainty ($\sigma_s < 0.1$mag) but also a good match between the observational calibration, the empirical formula proposed by Valenti et al. (2004) and our models; they are thus good candidates for obtaining a constraint on μ_ν: ω Centauri, 47 Tucanae, M3, M15, NGC 6255, 6273, 6304, 6440, 6569, Terzan 2 and Terzan 6. Eight allowed to place $\mu_{12} \leq 2.2$ as a fairly good upper limit for the magnetic dipole moment of neutrinos. However, in view of the possible uncertainties from both observations (due the sparsely populated RGB of most clusters) and stellar models (more recent physical ingredients suggest lighter helium cores and lower tip-RGB luminosities), it was much more prudent to adopt $\mu_\nu \leq 2.6 \times 10^{-12} \mu_B$ as a more robust constraint.

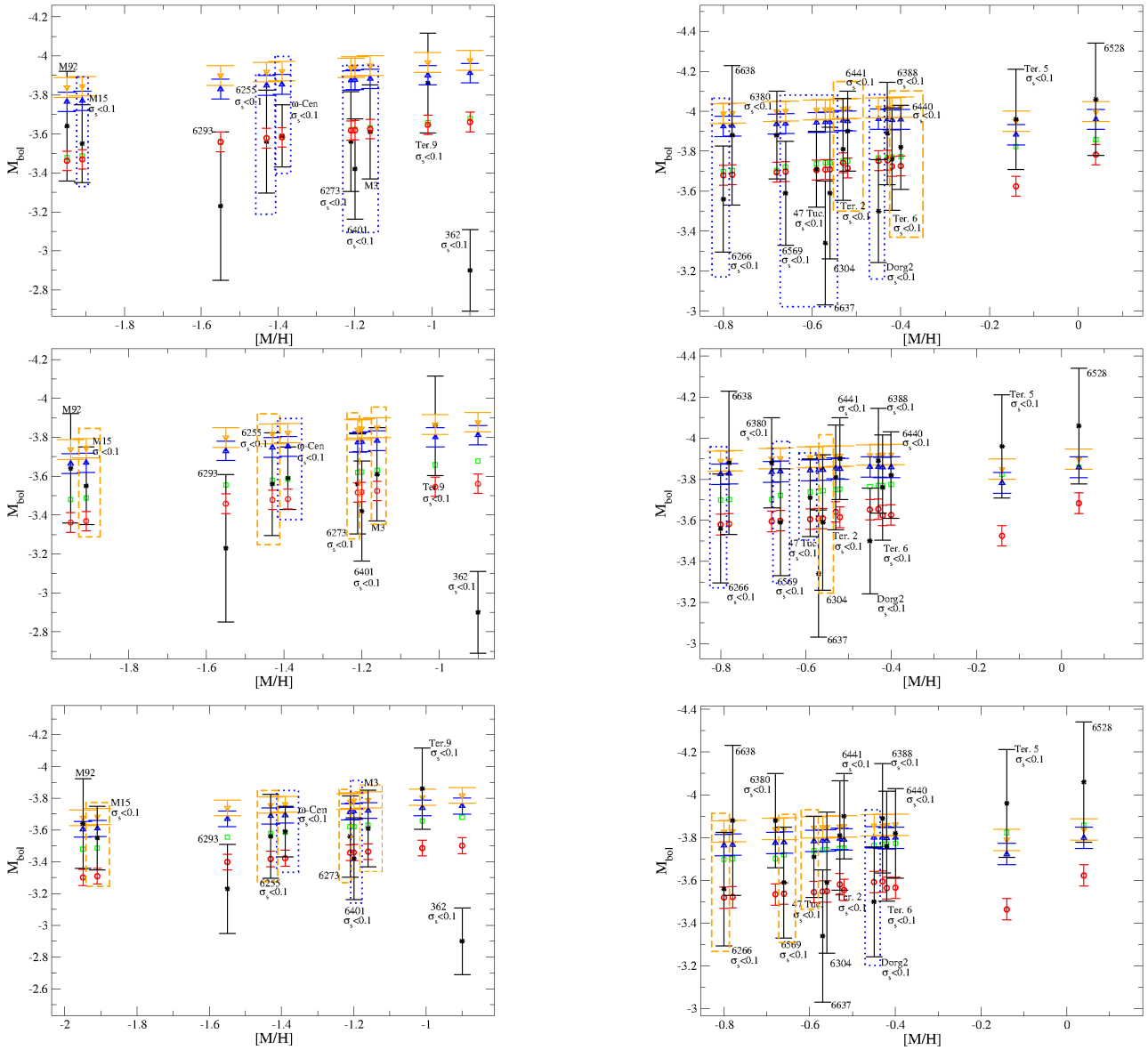

Fig. 3. Comparison between the observational tip-RGB (black asterisks), its empirical estimation (green squares) and our canonical (red circles) and non-standard models, with $\mu_{12} = 2.2$ (upward-blue triangles) and 2.6 (downward-orange triangles). In the two upper panels, twelve clusters (inside the blue boxes) were used to constrain $\mu_{12} \leq 2.2$. The lower panels show the results with shifts of 0.1 and 0.16 mag. The color figure can be viewed online.

3.2. *Qualitative analysis on specific NIR bands*

In addition to producing accurate estimations of bolometric corrections, the PHOENIX code offered us the advantage of constructing synthetic stellar spectra using stellar models as input. Although there were inaccuracies when calculating the effective temperature from the stellar evolution code our models were at least good enough to present a qualitative analysis of the absolute magnitude of specific spectral bands, when considering the effects on non-standard neutrino emission.

We selected the two brightest globular clusters in the galaxy for our study: ω Cen and 47 Tuc. The photometric data of these two clusters, presented by Bellazzini et al. (2004) and Sollima et al. (2004), are the most accurate to date on the tip-RGB measurements on specific bands on the near-infrared and were used to calibrate the tip-RGB bolometric luminosity and its counterparts on the I, J, H, and K

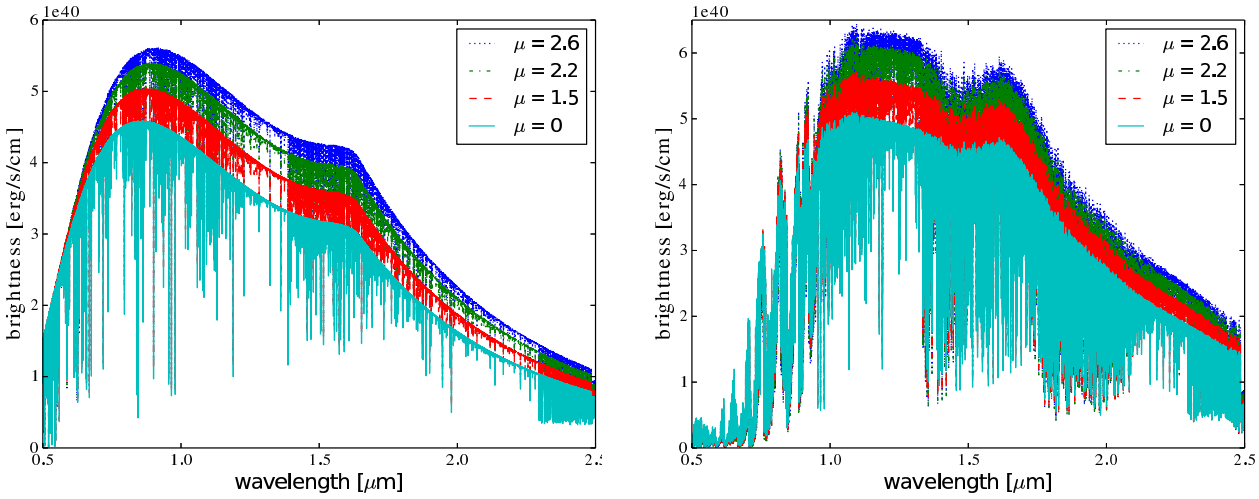

(a) NIR-spectra for ω-Cen.

(b) 47-Tucanae.

Fig. 4. Synthetic spectra and $\mu_{12} = 0$ to 2.6 (from top to bottom). Peak emission is on the I band and there is a bump at the center of the H band. The spectra for 47 Tuc are blurred out below $1\mu m$ by line blanketing. The region between the J and H bands shows the largest difference between the canonical and the non-standard scenarios, without being affected by metallicity. The color figure can be viewed online.

TABLE 6

BOLOMETRIC CORRECTIONS, ABSOLUTE MAGNITUDE, IN THE NIR-BANDS, FOR THE TIP-RGB OF ω-CEN AND THEIR DIFFERENCE FROM THE OBSERVATIONAL VALUES*

ω-Cen.	BC(I)	BC(J)	BC(H)	M_I	M_J	M_H	ΔM^{Tip}_{I-0}	ΔM^{Tip}_{J-0}	ΔM^{Tip}_{H-0}
$\mu_{12} = 0$	0.49	1.70	2.50	−4.04	−5.28	−6.08	+0.01	−0.08	−0.14
$\mu_{12} = 1$	0.46	1.70	2.52	−4.19	−5.43	−6.25	−0.15	−0.23	−0.31
$\mu_{12} = 2.2$	0.43	1.71	2.54	−4.28	−5.55	−6.39	−0.24	−0.35	−0.45
$\mu_{12} = 3$	0.41	1.72	2.56	−4.33	−5.64	−6.48	−0.29	−0.44	−0.54

*Reported values: $M_I^{Tip} = -4.05 \pm 0.12$, $M_J^{Tip} = -5.20 \pm 0.16$ and $M_H^{Tip} = -5.94 \pm 0.18$. The values for $\mu_{12} = 2.2$ lie more than 0.3 mag. away from the central value of observations.

bands as a function of global metallicity. We evolved the corresponding sets of stellar models (canonical and non-standard) up to their theoretical tip-RGB and used the resulting effective, temperatures and gravities to construct the stellar spectra. The results are presented in Tables 6, 7 and in Figure 4.

From our stellar models, we calculated bolometric corrections on the I, J and H bands and the resulting absolute magnitudes for ω Cen (Table 6) and 47 Tuc. (Table 7). We compared these values with the calibrations reported by Bellazzini et al. (2004) for each band. In all the spectral bands, the tip-RGB of models with $\mu_{12} = 2.2$ surpassed the upper limit of the observational calibration. Unlike bolometric luminosity, metallicity had an important effect on the magnitude of specific spectral bands. The I band in the synthetic spectra of 47 Tucanae (being almost 9 times more metallic than the main population in ω Cen) was highly affected by possible molecular lines on the stellar envelope, making the bolometric correction and the resulting absolute magnitude too inaccurate.

We show the synthetic spectra for both clusters in Figures 4a and 4b, units are erg·s^{-1}/cm, constructed with the PHOENIX code. We covered the range between 0.5 and 2.5 μm. In both cases, we found that the brightness in models with non-standard neutrino emission increased with larger values of μ_{12}. This resulted from the non-standard increase in luminosity, accompanied by a decrease of surface gravity (as a secondary effect driven by stellar expansion),

TABLE 7

SAME AS TABLE 6 BUT FOR 47 TUC*

47 Tuc.	BC(I)	BC(J)	BC(H)	M_I	M_J	M_H	ΔM^{Tip}_{I-0}	ΔM^{Tip}_{J-0}	ΔM^{Tip}_{H-0}
$\mu_{12}=0$	0.46	1.93	2.79	−4.17	−5.64	−6.50	0.26	−0.17	−0.15
$\mu_{12}=1$	0.59	1.95	2.81	−4.43	−5.79	−6.65	0.52	−0.32	−0.30
$\mu_{12}=2.2$	0.72	1.98	2.82	−4.66	−5.92	−6.76	0.75	−0.45	−0.41
$\mu_{12}=3$	0.80	1.99	2.83	−4.80	−5.99	−6.83	0.89	−0.52	−0.48

*The reported observational values are: $M^{Tip}_I = -3.91 \pm 0.13$, $M^{Tip}_J = -5.47 \pm 0.25$ and $M^{Tip}_H = -6.35 \pm 0.30$. Our estimation on the I band is not thrust worthy due to line blanketing (Figure 4).

due to the speeding-up of nuclear reactions inside the H-burning shell. We checked if changes of comparable size could be created in canonical models, by assuming pure changes in effective temperature, and found the changes to be very small compared to those caused by the increase in luminosity driven by non-standard plasmon decay. The synthetic spectra showed the emission peak on the I band and a bump on the center of the H band. This region, between 0.8 and 1.7 μm showed the largest difference between canonical and non-standard models. The influence of metallicity on the spectra of 47 Tuc was non-trivial for the bolometric correction of the I band. This region showed large gaps giving a quite different profile (unlike the case of our model for ω Cen, with a much lower metallicity). The spectral profile was less affected at larger wavelengths and the J band was probably the best suited for comparing the effect of non-standard neutrino emission in more accurate studies, as it showed a considerable difference between canonical and non-standard models and the effect of line blanketing was less pronounced.

4. DISCUSSION AND CONCLUSIONS

The existence of a non-zero magnetic dipole moment enhances the production of neutrinos by plasmon decay. This, as shown by our models, has several consequences for the conditions inside the stellar core, the energy loss channels and their evolution towards the tip-RGB:

- The existence of a non-zero magnetic dipole moment greatly affects the starting point and intensity of plasmon decay during stellar evolution (Figure 2). However, the associated changes in observable stellar parameters could only possibly be detected near the tip-RGB.
- The contribution of thermal processes to the total neutrino luminosity is much larger when considering a non-zero magnetic dipole moment for all our tip-RGB models, independently of metallicity; it was almost two times larger than with standard evolution. For our models with $\mu_{12} = 2.2$, the total neutrino luminosity is 20% larger, as a result of enhanced plasmon decay into neutrino pairs (Table 2).
- If mass-loss due to non-dust driven winds is taken into account, its rate should be calibrated to get the same total mass at the tip-RGB. Although the resulting envelope mass does not, in principle, affect the tip-RGB luminosity, the interaction between non-standard plasmon decay and surface gravity can suppress the helium flash if the mass-loss parameter is not properly calibrated. Our models with $\mu_{12} = 2.2$ require that η be reduced by about a 30%.
- We found that, independently of the initial stellar metallicity, the tip-RGB of any stellar track is reached around $L_{He} = 10 L_\odot$. Using models with matching chemical composition (§ 3), we compared this luminosity with the photometric data obtained by the group of Ferraro, Valenti & Origlia, for 24 globular clusters in the galactic bulge and halo), and that of Sollima et al. (2004) for ω Centauri. From these clusters, we got a bolometric magnitude around −3.65 and a non-standard $M^{Tip}_{bol} \approx -3.92$, around 0.25 mag higher, depending slightly on global metallicity.

Although we find twelve well populated globular clusters suggesting the constraint $\mu_\nu \leq 2.2 \times 10^{-12} \mu_B$ for the value of the neutrino magnetic dipole moment (with ω Centauri among those in which the statistical uncertainty is less than 0.1 mag) the current uncertainties in both observational data and stellar models cannot be ignored. While the statistical uncertainty can, in some way, be considered (by selecting clusters with RGB's as populated as possible), there are several

systematic factors in stellar models that would require a larger magnetic dipole moment to achieve a luminosity level high enough to get over the upper limits of the current error bars of observations: extreme helium enrichment (30% is enough by itself to transform our constraint to $\mu_{12} \leq 2.6$), the new opacities for electron conductivity (Cassisi et al. 2007), and the $N14 + p$ reaction rates (Weiss et al. 2005) can cause a similar effect (as we saw in Figure 3 by considering downward shifts of about 0.1 and 0.16 mag). This makes a $\mu_\nu \leq 2.6 \times 10^{-12}\mu_B$ a much more robust constraint, thus to be preferred.

REFERENCES

Adams, J. B., Ruderman, M. A., & Woo, C.-H. 1963, PhRv, 129

Alexander D. R. & Ferguson J. W. 1994, ApJ, 473, 879

Arceo-Díaz, S., Schröder, K.-P., & Zuber, K. 2013, ASP Conf. Ser., 472, 71

Arceo-Díaz, S., Schröder, K.-P., Zuber, K., & Jack D. 2014, RMxAC, 44, 147

Arceo-Diáz, S., Schröder, K.-P., Zuber, K., & Jack, D. 2015, Aph (accepted for its publication)

Beaudet, G., Petrosian, V. & Salpeter, E. E. 1967, ApJ, 307, L9

Beda, A. G., Brudanin, V. B., Egorov, V. G., et. al. 2013, PPNL, 10, 139

Bellazzini, M., Ferraro, F. R., Sollima, A., Pancino, E., & Origlia, L. 2004, A&A, 424, 199

Bernstein, J., Ruderman, M. & Feinberg, G. 1963, PhRv, 132, 1227

Castellani, M. & Castellani, V. 1993, ApJ, 407, 649

Cassisi S., Potekhin A. Y., Pietrinferni A., Catelan M., & Salaris M., 2007, ApJ, 661, 1094

Cranmer S. R.& Saar S. H., 2011, ApJ, 741, 54

Chen X. F. & Tout C. A. 2007, CJAA, 7, 245

Eggleton, P. 1971, MNRAS, 151, 351

Ferraro F. R., Montegrifo P., Origlia L., & Pecci F. F. 2000, AJ, 119, 1282

Ferraro F. R., Valenti E., & Origlia L. 2006, ApJ, 649, 243

Fujikawa K. & Shrock R. E. 1980, PhRvL, 45, 963

Haft, M., Raffelt, G. G., & Weiss, A. 1994, ApJ, 425, 222

Hauschildt, P. 1992, JQSRT, 47, 433

Iglesias C. A. & Rogers F. J. 1996, ApJ, 464, 943

Itoh, N., Adachi, T., Nakagawa, M., Kohyama, Y., & Munakata, H. 1989, ApJ, 339, 354; erratum 360, 741 (1990)

Itoh, N., Mutoh, H., Hikita, A., & Kohyama, Y. 1992, ApJ, 395, 622; erratum 404, 418 (1993)

Itoh, N., Hayashi, H. & Nishikawa, A. 1996, ApJSS, 102, 411

Hilker, M. & Richtler, T. 2000, A&A, 362, 895

Johnson, C. I. & Pilachowski, C. A. 2010, ApJ, 722, 1373

Kantor E. M. & Gusakov M. E. 2007, MNRAS, 381, 1702

Kippenhahn R. & Weigert A. 1990, Stellar Structure and Evolution, Springer Verlag, (Berlin)

Lee, B. W. & Shrock, R. E. 1977, PhRv, 16, 144

Marciano, W. J. & Sanda, A. I. 1977, PhL, 67, 303

Marino, A. F., Villanova, S., Piotto, G., Milone, A. P., Momany, Y., Bedin, L. R., & Medling, A. M. 2008, A&A, 490, 625

Montegriffo, P., Ferraro, F. R., Origlia, L., & Fusi Pecci, F. 1998, MNRAS, 297, 872

Norris, J. E. & Da Costa, G. S. 1995, ApJ, 447, 680

Pancino, E., Seleznev, A., Ferraro, F. R., Bellazzini, M., & Piotto, G. 2003, MNRAS, 345, 683

Pietrinferni, A., Cassisi S., Salaris, M., & Castelli, F. 2004, ApJ, 612, 168

Pietrinferni, A., Cassisi S., Salaris, M., & Castelli, F. 2006, ApJ, 642, 797

Pols, O., Tout, O. & Eggleton, P. P. 1995, MNRAS, 274, 964

Pols, O., Tout, C. A., Schröder, K.-P., Eggleton, P. P., & Manners, J. 1997, MNRAS, 289, 869

Pols, O., Schröder, K.-P., Hurley, J. R., & Tout, C. A. 1998, MNRAS, 298, 525

Raffelt G. G. & Dearborn D. S. P. 1988, PhRv, 37, 2

Raffelt G. G. 1990, ApJ, 365, 559

_____. 1990, PhRvL, 64, 24

Raffelt G. G. & Weiss A. 1992, A&A, 264, 536

Salaris M., Cassisi S., & Weiss A. 2002, PASP, 114, 375

Schröder, K.-P., Pols, O. R., & Eggleton, P. P. 1997, MNRAS, 285, 696

Schröder, K.-P. & Cuntz, M. 2005, ApJ, 630, 1, L73

_____. 2007, A&A, 465, 593

Sollima A., Ferraro F. R., Origlia L., Pancino E., & Bellazzini M. 2004, A&A, 420, 173

Sollima, A., Ferraro, F. R., Pancino, E. & Bellazzini M. 2005, MNRAS, 357, 265

Suntzeff, N. B. & Kraft, R. P. 1996, AJ, 111, 1913

Valcarce, A. A. R., Catelan, M., & Sweigart, A. V. 2012, A&A, 547, A5

Valenti, E., Ferraro F. R., & Origlia, L. 2004a, MNRAS, 351, 1204

_____. 2004b, MNRAS, 354, 815

_____. 2007, AJ, 133, 815

_____. 2010, MNRAS, 402, 1729

Viaux, N., Catelan, M., Stetson, P. B., Raffelt, G. G., Redondo, J., Valcarce, A. A. R., & Weiss, A. 2013, A&A, 558

Weiss, A., Serenelli, A., Kitsikis, A., Schlattl, H., & Christensen-Dalsgaard, J. 2005, A&A, 441, 1129

S. Arceo-Díaz, K.-P. Schröder, and D. Jack: Departamento de Astronomía, Universidad de Guanajuato
K. Zuber: Institut für Kern- und Teilchenphysik